Thin Solid Films 550 (2014) 700–704

Contents lists available at ScienceDirect

Thin Solid Films

journal homepage: www.elsevier.com/locate/tsf

Thin film solar cell based on $CuSbS_2$ absorber fabricated from an electrochemically deposited metal stack

Wilman Septina, Shigeru Ikeda *, Yuta Iga, Takashi Harada, Michio Matsumura

Research Center for Solar Energy Chemistry, Osaka University, 1-3 Machikaneyama, Toyonaka Campus, Osaka 560-8531, Japan

ARTICLE INFO

Article history:
Received 25 April 2013
Received in revised form 8 November 2013
Accepted 12 November 2013
Available online 20 November 2013

Keywords:
$CuSbS_2$
Solar cell
Electrodeposition
Preheating effects
Sulfurization

ABSTRACT

Copper antimony sulfide ($CuSbS_2$) thin films were fabricated by sulfurization of an electrodeposited metallic stack composed of Cu and Sb on a Mo-coated glass (Mo/glass) substrate. A $CuSbS_2$ film containing appreciable impurity components was obtained when the precursor metallic stack was heated monotonically from room temperature to 450 °C in Ar followed by sulfurization. The film also showed poor adherence due to a large number of crevices; there were many appreciable pinholes over the entire surface of the film. On the other hand, a $CuSbS_2$ film without any impurity phases was obtained when the metallic precursor film was pretreated at 510 °C in Ar for 60 min just before sulfurization at 450 °C. It was also observed that the thus-obtained $CuSbS_2$ film showed good adhesion to the Mo/glass substrate and almost no notable pinholes. As expected from structural analyses, the 510 °C-pretreated film worked as a relatively efficient absorber for the thin film solar cell with an Al:ZnO/CdS/$CuSbS_2$/Mo/glass structure: it gave preliminary conversion efficiency of 3.1%.

1. Introduction

Thin film solar cells based on the chalcogenide absorbers CdTe and $Cu(In,Ga)(Se,S)_2$ (CIGS) have reached highest energy conversion efficiencies of 16.5% and 20.3%, respectively [1,2]. These devices are currently being produced in a gigawatt range, which is comparable to the crystalline silicon-based devices. However, the toxicity of Cd and the scarcity of Te, In, and Ga are major problems limiting the widespread utilization of these devices.

Among the ongoing investigated absorber materials, $Cu_2ZnSn(S,Se)_4$ (CZTSSe) has attracted considerable attention because all of the constituent elements in CZTSSe have low toxicity and are naturally abundant [3,4]. The material has a tunable band gap energy (E_g) ranging from 1.0 eV for pure selenide to 1.5 eV for pure sulfide by changing the compositional ratio of Se to S [5–7]. It also has a high optical absorption coefficient of more than 10^4 cm^{-1} [8]. The current energy conversion efficiency of devices based on the CZTSSe material has advanced to 11.1% [9]. Since the value still lags behind those of CdTe- and CIGS-based devices, there are challenges in the CZTS system to achieve a high conversion efficiency of more than 15%.

Alternative ternary copper sulfides based on Cu–Sb–S and Cu–Bi–S materials such as $CuSbS_2$ and $CuBiS_2$ are expected to become promising absorber materials for sustainable and scalable photovoltaics because of their optimal E_gs (1.52 eV for $CuSbS_2$ and 1.65 eV $CuBiS_2$) as well as their abundant elements with low toxicity compared to those of CdTe and CIGS [10,11]. Recent theoretical studies have also predicted that these materials have strong optical absorption with absorption coefficients of more than 10^4 cm^{-1} [12], which is comparable to the above chalcopyrite and kesterite materials. Hence, various fabrication methods, such as thermal evaporation [13,14], and non-vacuum methods, such as chemical bath deposition (CBD) [15,16], spray pyrolysis [17] and electrodeposition [18,19], have been reported for fabrication of these I–V–VI chalcogenide thin films. However, only one study showed the application of these thin films to a complete device: the device based on $CuSbS_2$ showed low photovoltaic performance (open-circuit voltage (V_{OC}) of 345 mV and a short circuit current (J_{SC}) of 0.2 mA/cm^2), probably due to the less-crystalline nature of the $CuSbS_2$ film used [16].

An electrochemical approach is a desirable method for the fabrication of various chalcogenide thin films because of its advantages including low equipment cost, metal utilization rates close to 100% with bath recycling, possible formation of a compact film required for solar cell application, scalability, and manufacturability of a large-area polycrystalline film [20–29]. A previous work by our group showed that a similar method can be used to fabricate $CuInS_2$ and Cu_2ZnSnS_4 thin films [30–32]. These facts and results motivated us to investigate the production of these I–V–VI chalcogenide films through an electrochemical route for the use of efficient absorbers for solar cells. In this study, we therefore attempted to fabricate a promising I–V–VI chalcogenide thin-film absorber of $CuSbS_2$. Structural and morphological properties related to solar cell performances are discussed in detail.

2. Experimental

Metallic Cu and Sb layers were electrochemically deposited under potentiostatic control using a Hokuto Denko HSV-100 potentiostat–galvanostat. A three-electrode setup consisting of a Mo-coated glass

* Corresponding author. Tel.: +81 6 6850 6695; fax: +81 6 6850 6699.
E-mail address: sikeda@chem.es.osaka-u.ac.jp (S. Ikeda).

0040-6090/$ – see front matter © 2013 Elsevier B.V. All rights reserved.
http://dx.doi.org/10.1016/j.tsf.2013.11.046

working electrode, a platinum sheet counter electrode, and an Ag/AgCl reference electrode was used for the deposition. Deposition of Cu was performed at a potential of −0.4 V (*vs.* Ag/AgCl) in an electrolyte containing 15 mM $CuSO_4$ and 15 mM citric acid. Then the Sb layer was deposited at a potential of −0.3 V *vs.* Ag/AgCl from an electrolyte containing 15 mM $K_2(Sb_2(C_4H_2O_6)_2$ and 50 mM tartaric acid, with pH adjusted to 1.3 by the addition of H_2SO_4. During the deposition, the temperature of the electrolyte was kept at 25 °C by using a water bath. The amount of each deposited metal was fixed by controlling the electric charge during deposition using a Hokuto Denko HF-201A coulomb/amperehour meter: electric charges for depositions of Cu and Sb were maintained at 0.74 C/cm^2 and 1.1 C/cm^2, respectively, *i.e.*, the atomic ratio of Cu/Sb was fixed to be unity.

The stacked metal precursor was then sulfurized at 450 °C for 30 min under H_2S (5% in Ar) flow to form $CuSbS_2$ (CAS(A)). We also performed sulfurization of the precursor using a different heating profile, *i.e.*, the stacked metal precursor was heated at 510 °C for 60 min under argon (Ar) and then subsequently sulfurized at 450 °C for 30 min under a flow of 5% H_2S; the thus-obtained $CuSbS_2$ film was labeled CAS(B). Morphologies of the films were examined by scanning electron microscopy (SEM) using a Hitachi S-5000 FEG scanning electron microscope operated at 20 kV. Crystal structures of the films were measured by X-ray diffraction (XRD) using a Rigaku Mini Flex X-ray diffractometer in Bragg–Brentano mode (θ–2θ configuration) with Cu Kα radiation (30 kV, 15 mA) and Ni filter.

For the evaluation of solar cell properties of $CuSbS_2$ films, the films were processed to form an Al:ZnO/CdS/$CuSbS_2$/Mo/glass structure. After immersion of the $CuSbS_2$ films in an aqueous KCN solution (10%) for 2 min to clean their surfaces, a CdS buffer layer was deposited by chemical bath deposition (CBD). Then an Al:ZnO transparent conductive oxide was deposited on the top of the CdS layer by radio frequency (RF) magnetron sputtering. Current density-voltage (*J*–*V*) characteristics of thus-obtained devices under simulated AM1.5 irradiation (100 mW cm^{-2}) through the Al:ZnO window layer and those under the dark (without photoirradiation) were measured with a Bunkoh-Keiki CEP-015 photovoltaic measurement system.

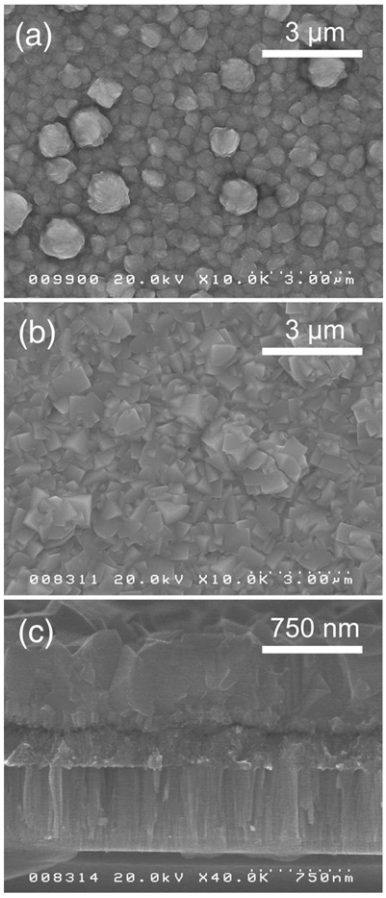

Fig. 1. SEM images of an electrodeposited (a) Cu layer and (b, c) a Cu/Sb stacked layer.

3. Results and discussion

Fig. 1 shows SEM images of the electrodeposited Cu layer and the Cu/Sb stacked layer. It is clearly shown that the Cu-layer was dense and consisted of round-shaped grains with sizes less than 1 μm (Fig. 1a). Upon electrodeposition of the Sb layer on the top of the Cu-layer (see Fig. 1b), the Sb layer homogenously covered the underlying Cu surface, as can be seen from the appearance of angular-shaped grains on the whole surface of the film. The Sb deposition resulted in a change of the color of the film from a metallic-orange (Cu-like color) to a metallic-gray (Sb-like color). The corresponding cross-sectional image (see Fig. 1c) clearly showed almost complete coverage of a rough Sb layer on the top of the homogeneous Cu-layer with thicknesses of the layers being *ca.* 0.3 μm and 0.85 μm, respectively.

The XRD pattern of the metallic stack after sulfurization at 450 °C for 30 min under an H_2S flow (*i.e.*, the CAS(A) film) indicated conversion of the film into a $CuSbS_2$ compound (JCPDS 44-1417) as shown in Fig. 2a. However, there were appreciable reflections assignable to Sb_2S_3 (JCPDS 42-1393) and an unidentified peak at 2θ of 44.5°. An extension of sulfurization duration and an increase in sulfurization temperature were not effective to eliminate these impurities: since such changes in the sulfurization profile often induced peeling-off of the film from the Mo/glass substrate, we could not perform systematical investigations of sulfurization parameters by using these simple sulfurization profiles. In order to reduce the formation of impurity phases and peeling-off, we added a preheating treatment at 510 °C for 30 min under Ar just before the sulfurization. Fig. 2b shows the XRD pattern of the thus-obtained film (CAS(B)). Except for the unidentified peak at 2θ of 44.5°, all of the reflections of the CAS(B) film were assigned to $CuSbS_2$, *i.e.*, the formation of the Sb_2S_3 phase could be avoided by applying such a preheating treatment.

Fig. 3 shows SEM images of CAS(A) and CAS(B). While the top-view SEM image of CAS(A) shows the formation of densely packed micron-sized grains, the film also contained appreciable pinholes between these grains, as shown in Fig. 3a. Moreover, the corresponding cross section clearly shows the presence of significant voids at the interface between the CAS(A) film and the Mo/glass substrate (Fig. 3b). Compared to the CAS(A) film, the $CuSbS_2$(B) film had a dense morphology and relatively large and homogenous grain sizes compared to those of the $CuSbS_2$(A) film: there were no pinholes on the surface of the $CuSbS_2$(B) film (Fig. 3c). Moreover, as shown in Fig. 3d, the cross-sectional image of the $CuSbS_2$(B) film shows relatively good adhesion to the Mo substrate and almost no appreciable voids which were observed in the CAS(A) film.

In order to examine the effect of pretreatment at 510 °C in Ar, structural changes of the Cu/Sb metallic stack were evaluated by XRD analyses. Fig. 4 shows the results. The XRD pattern of the Cu/Sb stacked film before 510 °C-pretreatment consisted of a mixture of metallic Sb (JCPDS 35-0732), Cu (JCPDS 04-0836) and Cu_2Sb compound (JCPDS 87-1176), as shown in Fig. 4a. The presence of the Cu_2Sb compound in the as-deposited film indicates an appreciable interdiffusion between Cu and Sb during electrochemical coverage with Sb at room temperature. In fact, the phase diagram of this binary compound implies the preferable formation of the Cu_2Sb phase at temperatures below 526 °C, when the atomic ratio of Cu to Sb is less than 2 [33]. Upon heating the stacked layer at 510 °C in Ar, the Cu_2Sb reflections became more intense and well-resolved, indicating a significant intermixing of the metals and the formation of crystalline Cu_2Sb, although a minor trace from an unmixed Sb was still detected (Fig. 4b).

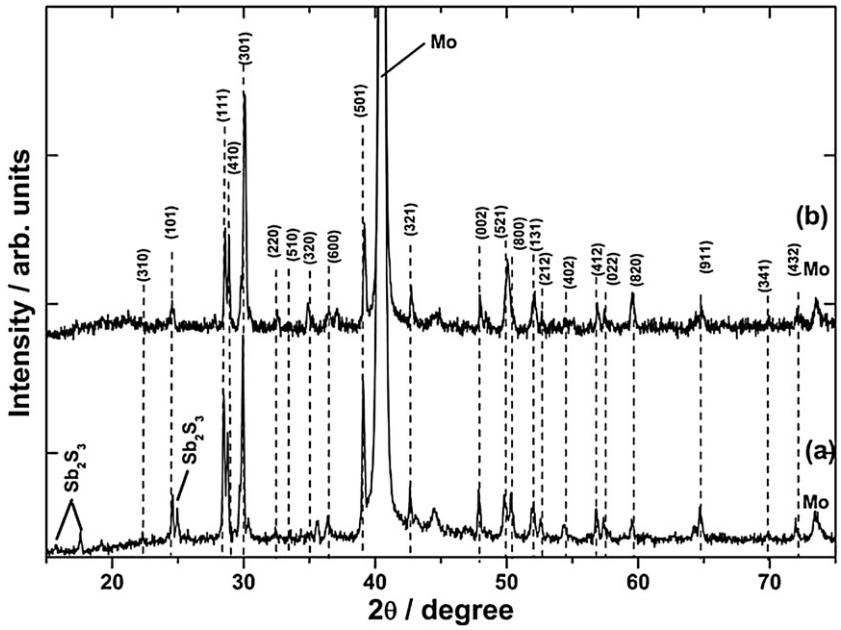

Fig. 2. XRD patterns of (a) CAS(A) and (b) CAS(B). Vertical indexed lines correspond to the Bragg reflections of $CuSbS_2$ (JCPDS 44-1417).

As has been discussed previously regarding sulfurization of Cu/In and Cu/Sn/Zn metallic stacks for fabrication of $CuInS_2$ and Cu_2ZnSnS_4 thin films [30,32], formation of significant voids between these chalcogenide thin-films and the Mo/glass substrate was due to a preferable reaction between Cu and sulfur vapor to produce a Cu_xS compound. The reaction would induce out-diffusion of the bottom Cu component to the surface, leading to an empty space remaining at the bottom part of the film. Moreover, the preferable Cu_xS formation might also induce inhomogeneous distribution of the Cu component, resulting in insufficient grain growth of the $CuSbS_2$ phase, formation of the Sb_2S_3 secondary phase, and production of appreciable pinholes between these grains. When 510 °C pretreatment of Ar was added to the Cu/Sb precursor, however, the formation of the Cu_xS compound could be suppressed by the formation of a Cu_2Sb alloy, which would suppress the preferential reaction between metallic Cu and sulfur vapor. Instead, relatively reactive or unstable sulfurized compounds were probably formed from the Cu_2Sb alloy; their conversion into the $CuSbS_2$ phase occurred promptly.

The $CuSbS_2$ films were transferred into devices with a structure of Al:ZnO/CdS/$CuSbS_2$/Mo/glass. Fig. 5 shows *J–V* curves of the devices. It is evident from the curves that all of the devices exhibited solar cell performance. Best conversion efficiencies of 1.24% (J_{SC}: 10.27 mA/cm^2, V_{OC}: 0.37 V, FF: 0.33) and 3.13% (J_{SC}: 14.73 mA/cm^2, V_{OC}: 0.49 V, FF: 0.44) were achieved from the devices using CAS(A) and CAS(B) films, respectively. It is apparent that all of the solar cell properties of the CAS(B)-based device were superior to those of the CAS(A)-based device. Differences in the solar cell properties could be related to the above-discussed

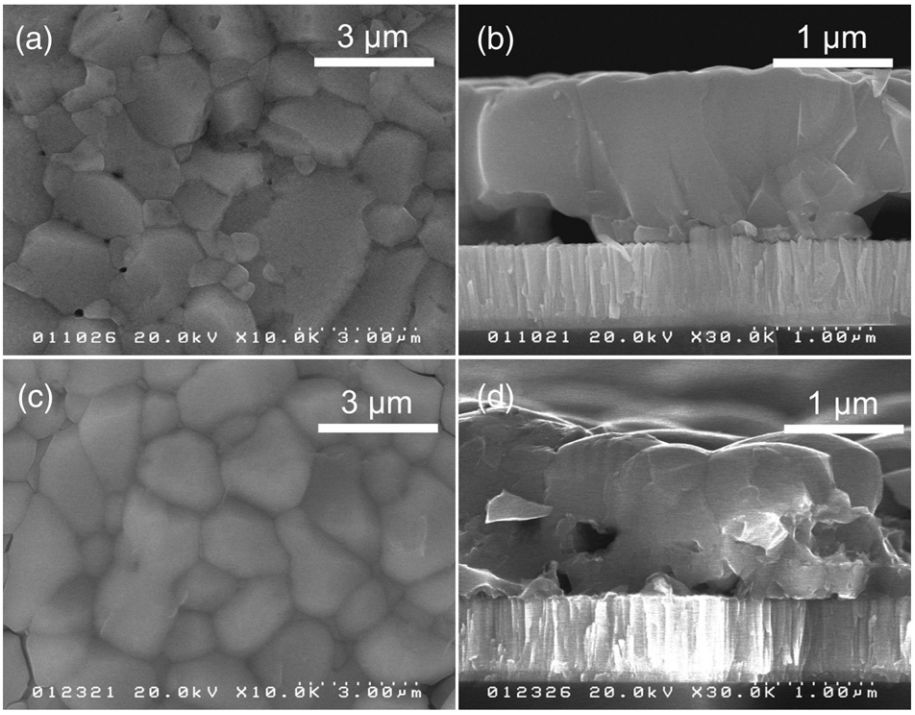

Fig. 3. Top view (a, c) and cross-sectional SEM images of (a, b) CAS(A) and (c, d) CAS(B).

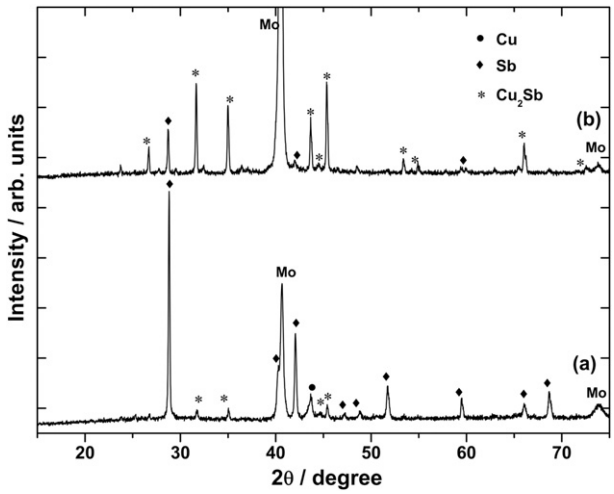

Fig. 4. XRD patterns of (a) an electrodeposited Cu/Sb stacked layer and (b) that heated at 510 °C in Ar.

structural and morphological properties of the CAS(B) film. For example, due to the improvement of adhesion to the Mo/glass substrate, the CAS(B)-based device should decrease interfacial resistance between the $CuSbS_2$ film and the Mo/glass substrate. Elimination of pinholes in the CAS(B) film would suppress cell leakage. Moreover, the disappearance of the Sb_2S_3 secondary phase in the CAS(B) film might reduce carrier recombination probability.

Fig. 6 shows the External Quantum Efficiency (EQE) spectrum of the best device (*i.e.*, the CAS(B)-based device). There are several features and problems of the present device. First, a significant loss of the EQE at a wavelength shorter than ca. 550 nm was observed due to the photoabsorption by transparent conductive oxide (Al:ZnO, Eg = 3.3 eV) and n-type buffer (CdS, Eg = 2.4 eV) layers in the present device. Second, there is also a non-linear decrease in EQE at a wavelength longer than ca. 550 nm, *i.e.*, EQE gradually decreases in wavelengths between ca. 550 nm and ca. 650 nm, becomes flat at wavelengths up to *ca.* 750 nm, and then again decreases steeply to onset wavelengths of *ca.* 850 nm, corresponding to the band gap energy of $CuSbS_2$ (*ca.* 1.5 eV). As has been reported in the literature, the flattening of EQE at *ca.* 650–750 nm was caused by the optical characteristic of $CuSbS_2$ [12]. On the other hand, the overall gradual decrease of EQE in this region was likely to be due to the insufficient minority carrier diffusion length of the present $CuSbS_2$, as has been frequently observed in a CZTS-based solar cell [5]. In order to improve the conversion efficiency, therefore, further optimization of the properties/qualities of the $CuSbS_2$ film is required. Since the maximum EQE value of the present cell only reached 0.8

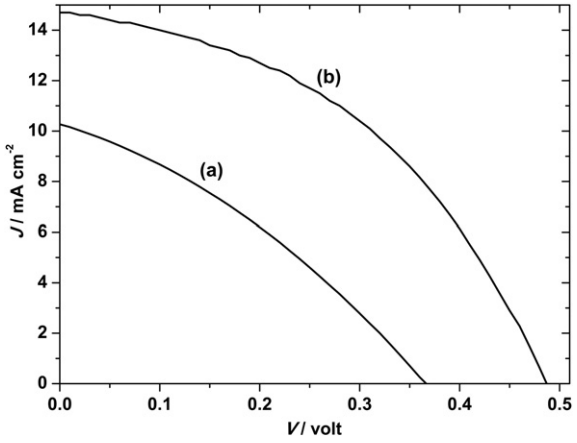

Fig. 5. *J–V* curves of Al:ZnO/CdS/$CuSbS_2$/Mo/Glass devices derived from (a) CAS(A) and (b) CAS(B).

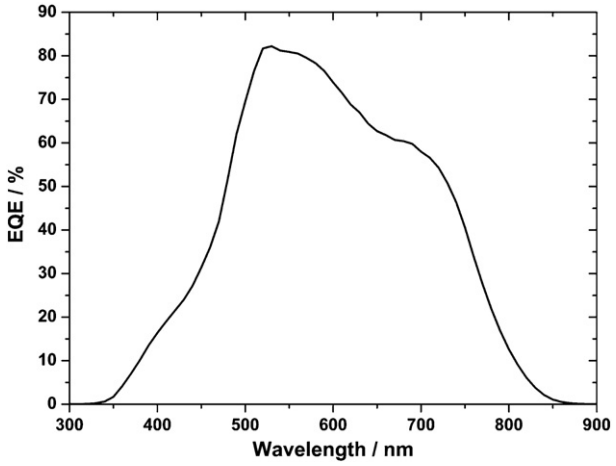

Fig. 6. EQE spectrum of the device derived from CAS(B).

(at 530 nm), moreover, improvements of junction properties (*i.e.*, optimization of materials and methods for deposition of an n-type layer) are also required.

4. Conclusion

In this study, we examined the fabrication of a $CuSbS_2$-based solar cell from electrodeposited Cu/Sb stacked layers followed by sulfurization at 450 °C in H_2S gas for 30 min. We found that the preheating under Ar to the stacked layer prior to sulfurization was beneficial for obtaining a $CuSbS_2$ film with a dense structure and good adherence to the Mo substrate. A maximum conversion efficiency of 3.13% has been achieved with the solar cell device using this approach. In order to improve the photovoltaic performance, various optimizations, such as sulfurization conditions, precise control of Cu/Sb atomic ratio, thickness of the $CuSbS_2$ film, and choice of optimum buffer layer, should be required. Hence, studies along with these lines are now in progress.

Acknowledgements

This work was carried out as part of a program supported by the New Energy and Industrial Technology Development Organization (NEDO). One of the authors (WS) would like to thank MEXT for providing a scholarship during the study. The authors also would like to thank Diego Colombara and Prof. Laurence M. Peter from the University of Bath, UK for their stimulating suggestions and discussions.

References

[1] X.X. Wu, Sol. Energy 77 (2004) 803.
[2] P. Jackson, D. Hariskos, E. Lotter, S. Paetel, R. Wuerz, R. Menner, W. Wischmann, M. Powalla, Prog. Photovolt. Res. Appl. 19 (2011) 894.
[3] L.M. Peter, Philos.Trans. Ser. A Math. Phys. Eng. Sci. 369 (2011) 1840.
[4] C. Wadia, A.P. Alivisatos, D.M. Kammen, Environ. Sci. Technol. 43 (2009) 2072.
[5] H. Katagiri, K. Saitoh, T. Washio, H. Shinohara, T. Ku-rumadani, S. Miyajima, Sol. Energy Mater. Sol. Cells 65 (2001) 141.
[6] T.M. Friedlmeier, H. Dittrich, H.W. Schock, Inst. Phys. Conf. Ser. 152 (1998) 345.
[7] S. Chen, A. Walsh, J.-H. Yang, X. Gong, L. Sun, P.-X. Yang, J.-H. Chu, S.-H. Wei, Phys. Rev. B 83 (2011) 125201.
[8] R. AdhiWibowo, E. Soo Lee, B. Munir, K. Ho Kim, Phys. Status Solidi A 204 (2007) 3373.
[9] T.K. Todorov, J. Tang, S. Bag, O. Gunawan, T. Gokmen, Y. Zhu, D.B. Mitzi, Adv. Energy Mater. 3 (2013) 34.
[10] J.T.R. Dufton, A. Walsh, P.M. Panchmatia, L.M. Peter, D. Colombara, M. Saiful Islam, Phys. Chem. Chem. Phys. 14 (2012) 7229.
[11] D.J. Temple, A.B. Kehoe, J.P. Allen, G.W. Watson, D.O. Scanlon, J. Phys. Chem. 116 (2012) 7334.
[12] L. Yu, R.S. Kokenyesi, D.A. Keszler, A. Zunger, Adv. Energy Mater. 3 (2013) 43.
[13] C. Garza, S. Shaji, A. Arato, E.P. Tijerina, G.A. Castillo, T.K. Das Roy, B. Krishnan, Sol. Energy Mater. Sol. Cells 95 (2011) 2001.
[14] A. Rabhi, M. Kanzari, B. Rezig, Mater. Lett. 62 (2008) 3576.
[15] Y. Rodriguez-Lazcano, M.T.S. Nair, P.K. Nair, J. Cryst. Growth 223 (2001) 399.
[16] Y. Rodriguez-Lazcano, M.T.S. Nair, P.K. Nair, J. Electrochem. Soc. 152 (2005) G635.

[17] S. Manolache, A. Duta, L. Isac, M. Nanu, A. Goossens, J. Schoonman, Thin Solid Films 515 (2007) 5957.
[18] D. Colombara, L.M. Peter, K.D. Rogers, J.D. Painter, S. Roncallo, Thin Solid Films 519 (2011) 7438.
[19] D. Colombara, L.M. Peter, K.D. Rogers, K. Hutchings, J. Solid State Chem. 186 (2012) 36.
[20] D. Lincot, J.F. Guillemoles, S. Taunier, D. Guimard, J. Sicx-Kurdi, A. Chaumont, O. Roussel, O. Ramdani, C. Hubert, J.P. Fauvarque, N. Bodereau, L. Parissi, P. Panheleux, P. Fanouillere, N. Naghavi, P.P. Grand, M. Benfarah, P. Mogensen, O. Kerrec, Sol. Energy 77 (2004) 725.
[21] A. Duchatelet, G. Savidand, R.N. Vannier, E. Chassaing, D. Lincot, J. Renewable Sustainable Energy 5 (2013) 011203.
[22] D.-C. Nguyen, S. Tanaka, H. Nishino, K. Manabe, S. Ito, Nanoscale Res. Lett. 8 (2013), http://dx.doi.org/10.1186/1556-276X-8-8.
[23] S.M. Pawar, B.S. Pawar, K.V. Gurav, D.W. Bae, S.H. Kwon, S.S. Kolekar, J.H. Kim, Jpn. J. Appl. Phys. 51 (2012)(art. No. 10NC27).
[24] J.J. Scragg, D.M. Berg, P.J. Dale, J. Electroanal. Chem. 646 (2010) 52.
[25] A. Ennaoui, M. Lux-Steiner, A. Weber, D. Abou-Ras, I. Kotschau, H.W. Schock, R. Schurr, A. Holzing, S. Jost, R. Hock, T. Voss, J. Schulze, A. Kirbs, Thin Solid Films 517 (2009) 2511.
[26] L. Guo, Y. Zhu, O. Gunawan, T. Gokmen, V.R. Deline, S. Ahmed, L.T. Romankiw, H. Deligianni, Prog. Photovolt. Res. Appl. (2013), http://dx.doi.org/10.1002/pip.2332.
[27] S. Ahmed, K.B. Reuter, O. Gunawan, L. Guo, L.T. Romankiw, H. Deligianni, Adv. Energy Mater. 2 (2012) 253.
[28] W. Septina, S. Ikeda, A. Kyoraiseki, T. Harada, M. Matsumura, Electrochim. Acta 88 (2013) 436.
[29] W. Septina, S. Ikeda, T. Harada, M. Matsumura, physic. status solidi (c) 10 (2013) 1062.
[30] S.M. Lee, S. Ikeda, T. Yagi, T. Harada, A. Ennaoui, M. Matsumura, Phys. Chem. Chem. Phys. 13 (2011) 6662.
[31] S.M. Lee, S. Ikeda, Y. Otsuka, T. Harada, M. Matsumura, Electrochim. Acta 79 (2012) 189.
[32] Y. Lin, S. Ikeda, W. Septina, T. Harada, Michio Matsumura, Sol. Energy Mater. Sol. Cells (2013), http://dx.doi.org/10.1016/j.solmat.2013.09.006.
[33] X. Liu, C. Wang, I. Ohnuma, R. Kainuma, K. Ishida, J. Phase Equilib. 21 (2000) 432.